Characterization of negative refraction with multilayered mushroom-type metamaterials at microwaves

Chandra S. R. Kaipa,[1,a)] Alexander B. Yakovlev,[1] and Mário G. Silveirinha[2]
[1]*Department of Electrical Engineering, The University of Mississippi, University, Mississippi 38677-1848, USA*
[2]*Departamento de Engenharia Electrotécnica, Instituto de Telecomunicações, Universidade de Coimbra Pólo II, 3030-290 Coimbra, Portugal*

(Received 22 September 2010; accepted 13 December 2010; published online 23 February 2011)

In this paper, it is shown that bulk metamaterials formed by multilayered mushroom-type structures enable broadband negative refraction. The metamaterial configurations are modeled using homogenization methods developed for a uniaxial wire medium loaded with periodic metallic elements (for example, patch arrays). It is shown that the phase of the transmission coefficient decreases with the increasing incidence angle, resulting in the negative spatial shift of the transmitted wave. The homogenization model results are obtained with the uniform plane-wave incidence, and the full-wave results are generated with a Gaussian beam excitation, showing a strong negative refraction in a significant frequency band. Having in mind a possible experimental verification of our findings, we investigate the effect of introducing air gaps in between the metamaterial layers, showing that even in such simple configuration the negative refraction phenomenon is quite robust. © *2011 American Institute of Physics*. [doi:10.1063/1.3549129]

I. INTRODUCTION

Negative-index metamaterials have been the subject of interest in recent years, due to their extraordinary properties such as, partial focusing, sub-wavelength imaging, and negative refraction. In particular, the phenomenon of negative refraction has attracted attention both in the optical and microwave communities. This phenomenon can in general be observed in materials with simultaneously negative permittivity and permeability, as originally suggested by Veselago.[1] However, the emergence of negative refraction due to a negative phase velocity has been reported much earlier by Schuster[2] and Mandelshtam.[3] Although, negative refraction is not observed in conventional dielectrics, the advent of metamaterials brought new opportunities to observe this phenomenon, as reported recently in the literature.

In Refs. 4–6, negative refraction has been realized using the materials with indefinite anisotropic properties, in which not all the principal components of the permittivity and permeability tensors have the same sign. Also, some other possibilities include the use of a nonlocal material formed by a crossed wire mesh, which results in broadband negative refraction,[7] and by engineering the dispersion of the photonic crystals.[8] Recently, negative refraction was also observed at optical frequencies by using an array of metallic nanorods.[9,10] However, the design considered in Refs. 9 and 10 is effective only at optical frequencies. At lower THz and microwave frequencies the array of nanorods is characterized by strong spatial dispersion,[11] and it behaves very differently from a material with indefinite properties.

However, it has been recently shown that the spatial dispersion (SD) effects in wire medium, formed by a two-dimensional lattice of parallel conducting wires, can be significantly reduced.[12–14] In Ref. 12, it was suggested coating the wires with a magnetic material or attaching large conducting plates to the wires. In Refs. 13 and 14, it has been shown based on nonlocal and local homogenization models that the periodic metallic vias in the mushroom structure can be treated as a uniaxial continuous Epsilon-Negative (ENG) material loaded with a capacitive grid of patches, with a proper choice of the period and the thickness of the vias. Based on these findings, it has been shown in Refs. 15 and 16 that by periodically attaching metallic patches to an array of parallel wires (with the unit cell resembling in part the mushroom structure) it is possible to synthesize a multilayered local uniaxial ENG material at longer wavelengths loaded with patch arrays.

In this work, as a continuation of our preliminary study in Refs. 15 and 16, we show that by periodically attaching metallic patches to an array of metallic wires (when SD effects are significantly reduced) it is possible to mimic the observed phenomenon of negative refraction from an array of metallic nanorods at optical frequencies, in the microwave regime. We present a complete parametric study of the negative refraction effect, highlighting its dependence on frequency, thickness of the metamaterial slab, and show how it can be conveniently modeled using effective medium theory. In addition, we investigate the effect of introducing air gaps in between the different metamaterial layers [formed by periodically attaching pairs of metallic patches to an array of metallic vias embedded in a single dielectric slab] aiming at a possible experimental verification of our findings, and show that such simple configuration enables the control of the negative refraction angle. The propagation characteristics in the proposed multilayered mushroom structures are analyzed using the nonlocal and local homogenization models for the wire medium (WM). Our results show that there is an excellent agreement between the two homogenization models over a wide frequency range, which demonstrates, indeed,

a)Author to whom correspondence should be addressed. Electronic mail: ckaipa@olemiss.edu.

the suppression of SD effects in the WM. The numerical results are presented for several configurations (with and without the air gaps) showing a broadband strong negative refraction at microwave frequencies.

The paper is organized as follows. In Sec. II, the formalism of nonlocal and local homogenization models is presented for a multilayered mushroom-type metamaterial. Section III focuses on the analysis of negative refraction in the proposed configurations with the plane-wave incidence and Gaussian beam excitation. In particular, the structure with air gaps is of practical interest, wherein the angle of negative refraction can be controlled. The conclusions are summarized in Sec. IV.

II. HOMOGENIZATION OF MULTILAYERED MUSHROOM-TYPE METAMATERIAL

The multilayered mushroom structure is formed by the grids of metallic square patches separated by dielectric slabs perforated with metallic pins (vias) connected to the metallic elements. The geometry of the structure with a transverse magnetic (TM) plane-wave incidence is shown in Fig. 1. Here, a is the period of the patches and the vias, g is the gap between the patches, h is the thickness of the dielectric layer between the patch arrays, ε_h is the permittivity of the dielectric slab, and r_0 is the radius of the vias.

In our analytical model, the dielectric slabs perforated with vias are modeled as WM slabs, and the patch arrays are treated as homogenized surfaces with the capacitive grid impedance obtained from the effective circuit parameters for subwavelength elements.[17] For completeness, we consider two different homogenization models (nonlocal and local) for the wire medium as described in the sections to follow, with the aim of demonstrating that in the proposed multilayered configuration (Fig. 1) the SD effects are significantly reduced. A time dependence of the form $e^{j\omega t}$ is assumed and suppressed.

A. Nonlocal homogenization model

For long wavelengths the WM can be characterized by a spatially-dispersive model of a uniaxial material with the effective relative permittivity along the vias (Refs. 15 and 16, and references therein):

$$\varepsilon_{zz}^{nonloc}(\omega, k_z) = \varepsilon_h\left(1 - \frac{k_p^2}{k_h^2 - k_z^2}\right), \tag{1}$$

where $k_h = k_0\sqrt{\varepsilon_h}$ is the wave number in the host material, $k_0 = \omega/c$ is the free space wave number, ω is the angular frequency, c is the speed of light in vacuum, and k_z is the z-component of the wave vector $\vec{k} = (k_x, 0, k_z)$. In Eq. 1, k_p is the plasma wave number defined in Ref. 11 as $k_p = \sqrt{(2\pi/a^2)/[\log(a/2\pi r_0) + 0.5275]}$. It should be noted that the plasma wave number depends on the period and on the radius of the vias. The dependence of the permittivity on the wave vector is a consequence of the fact that the macroscopic electric displacement cannot be linked to the macroscopic electric field through a local relation. The nonlocal model predicts the propagation of TM and transverse electromagnetic (TEM) fields in the wire medium.[18] Suppose that a plane wave with the y-polarized magnetic field (TM polarization) is incident at an angle θ_i (with the plane of incidence chosen as the x-z plane) on the structure as shown in Fig. 1. Following Ref. 18, the electric and magnetic fields in the WM slab [with the nonlocal dielectric function (Eq. 1)] can be expressed in terms of waves propagating along opposite directions with respect to the z-axis:

$$\eta_0 H_y = A_{\mathrm{TM}}^{+}e^{+\gamma_{\mathrm{TM}}z} + A_{\mathrm{TM}}^{-}e^{-\gamma_{\mathrm{TM}}z} + B_{\mathrm{TEM}}^{+}e^{+\gamma_{\mathrm{TEM}}z} + B_{\mathrm{TEM}}^{-}e^{-\gamma_{\mathrm{TEM}}z}, \tag{2}$$

$$E_x = \frac{j}{\varepsilon_h k_0}\left[\gamma_{\mathrm{TM}}\left(A_{\mathrm{TM}}^{+}e^{+\gamma_{\mathrm{TM}}z} - A_{\mathrm{TM}}^{-}e^{-\gamma_{\mathrm{TM}}z}\right) + \gamma_{\mathrm{TEM}}\left(B_{\mathrm{TEM}}^{+}e^{+\gamma_{\mathrm{TEM}}z} - B_{\mathrm{TEM}}^{-}e^{-\gamma_{\mathrm{TEM}}z}\right)\right], \tag{3}$$

$$E_z = -\frac{k_x}{\varepsilon_{zz}^{\mathrm{TM}}k_0}\left(A_{\mathrm{TM}}^{+}e^{+\gamma_{\mathrm{TM}}z} + A_{\mathrm{TM}}^{-}e^{-\gamma_{\mathrm{TM}}z}\right), \tag{4}$$

where $\gamma_{\mathrm{TEM}} = jk_0\sqrt{\varepsilon_h}$, $\gamma_{\mathrm{TM}} = \sqrt{k_p^2 + k_x^2 - k_0^2\varepsilon_h}$, $k_x = k_0\sin\theta_i$ is the x-component of the wave vector $\vec{k}$, $\varepsilon_{zz}^{\mathrm{TM}} = \varepsilon_h k_x^2/(k_p^2 + k_x^2)$ is the relative permittivity along the vias for TM-polarization, and η_0 is the impedance of free space. Similarly, the fields associated with the reflected and transmitted waves in the air regions (above and below the multilayered structure) are obtained in terms of the reflection and transmission coefficients, R and T. At the patch grid interfaces (at the planes $z = z_0 = 0, -h, -2h, ..., -L$) the tangential electric and magnetic fields can be related via sheet admittance,

$$E_x = -\frac{1}{\mathrm{y}_g}\left(H_y|_{z=z_0^+} - H_y|_{z=z_0^-}\right) \tag{5}$$

with the E_x-component of the electric field continuous across the patch grid,

$$E_x|_{z=z_0^+} = E_x|_{z=z_0^-}. \tag{6}$$

In Eq. 5, y_g is the normalized effective grid admittance of the patch array,[17]

$$\mathrm{y}_g = -j\frac{1}{\eta_0}\varepsilon_{qs}k_0\frac{2a}{\pi}\ln\left[\csc\left(\frac{\pi g}{2a}\right)\right] \tag{7}$$

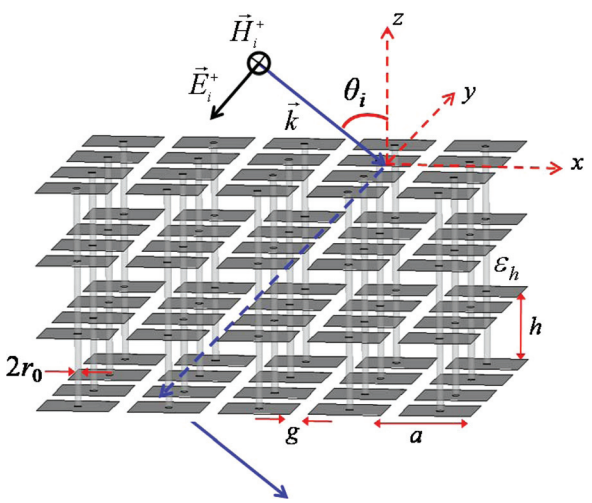

FIG. 1. (Color online) 3D view of a multilayered mushroom-type metamaterial formed by periodically attaching metallic patches to an array of parallel wires.

with $\varepsilon_{qs} = (\varepsilon_h + 1)/2$ for the lower and the upper external grids and $\varepsilon_{qs} = \varepsilon_h$ for all the internal grids. In order to find the unknown amplitudes $A^{\pm}_{\mathrm{TM}}$ and $B^{\pm}_{\mathrm{TEM}}$ associated with the TM and TEM fields in Eqs. 2–4 besides the boundary conditions Eqs. 5 and 6 at the patch interfaces, an additional boundary condition (ABC) is required at the connection of WM to the metallic patches. Following Refs. 13, 14 and 19, the ABC is associated with the zero charge density at the connection of metallic pins to the metallic elements of the capacitive patch arrays [equivalently for the microscopic current at the connection point, $dI(z)/dz = 0$], and is expressed in terms of the macroscopic field components,

$$k_0 \varepsilon_h \frac{dE_z}{dz} + k_x \eta_0 \frac{dH_y}{dz} = 0. \tag{8}$$

Using Eqs. 5, 6, and the ABC (Eq. 8), the reflected (at the upper interface) and the transmitted (at the lower interface) fields of the entire multilayered mushroom structure (Fig. 1) are related in the matrix form:

$$\begin{bmatrix} E_x \\ \eta_0 H_y \end{bmatrix}_{\text{lower interface}} = M_G \cdot \begin{bmatrix} E_x \\ \eta_0 H_y \end{bmatrix}_{\text{upper interface}} \tag{9}$$

where M_G is the global transfer matrix, which takes into account the product of the transfer matrices across the plane of metallic patches and for the propagation across the region in between two adjacent patch arrays (as WM slab). The analytical expressions of the transfer matrices are given in the Appendix.

The reflection and transmission coefficients, R and T, of the multilayered mushroom structure can be easily obtained from Eq. 9 by solving the following matrix equation

$$M_G \cdot \begin{bmatrix} \frac{j\gamma_0}{k_0} \\ -1 \end{bmatrix} R + \begin{bmatrix} \frac{j\gamma_0}{k_0} \\ 1 \end{bmatrix} T = M_G \cdot \begin{bmatrix} \frac{j\gamma_0}{k_0} \\ 1 \end{bmatrix}. \tag{10}$$

B. Local homogenization model

In the local homogenization model, the WM slab (as a uniaxial continuous ENG material) is characterized for long wavelengths by the classical Drude dispersion model, which does not take into account SD effects (Refs. 13 and 14, and references therein):

$$\varepsilon^{loc}_{zz}(\omega) = \varepsilon_h \left(1 - \frac{k_p^2}{k_h^2}\right). \tag{11}$$

This approximation is valid when the current along the vias is uniform (or for long vias at low frequencies when the WM can be characterized as a material with extreme anisotropy).[18] This assumption is justified because both ends of the vias are connected to the metallic elements of the patch arrays, and the charge is distributed over the surface of the metallic patches. Therefore, the charge density is approximately zero at the connection points and along the vias, and the field is nearly uniform in the WM slab.[18] Within the local model formalism, the amplitudes of the electric and magnetic field components in the WM slab are expressed as follows:

$$\eta_0 H_y = H^+ e^{+\gamma z} + H^- e^{-\gamma z}, \tag{12}$$

$$E_x = \frac{j\gamma}{\varepsilon_h k_0}(H^+ e^{+\gamma z} - H^- e^{-\gamma z}), \tag{13}$$

where γ is the propagation constant in the WM slab along the direction of the vias given in Refs. 13 and 14

$$\gamma = \sqrt{\frac{k_x^2}{\varepsilon^{loc}_{zz}} - k_h^2}. \tag{14}$$

The local model takes into account only the effect of frequency dispersion in the WM slab, and treats the WM as an ENG uniaxial continuous material below the plasma frequency. The local model does not require an ABC, as it does not take into account the SD effects in the WM.

The transmitted and reflected fields are related in a similar matrix form Eqs. 9 and 10, satisfying the classical boundary conditions for tangential electric and magnetic field components at interfaces (Eqs. 5 and 6). The analytical expressions of the transfer matrices used in the local model are given in the Appendix. It should be noted that the local homogenization model may predict accurately the response of the structure when the SD effects are significantly reduced (it will be shown in Section III, that this is the case in a multilayered mushroom structure).

III. RESULTS AND DISCUSSION

In this section, the transmission properties of the mushroom-type metamaterials are studied under the plane-wave incidence, using both the nonlocal and local homogenization models. The negative refraction effect is characterized from the obtained transmission properties. We consider two multilayered mushroom-type metamaterials: the first configuration is as shown in Fig. 1, and the second one is formed by the inclusion of air gaps (without vias) in between two-layered (paired) mushrooms (with the geometry shown in Fig. 6 later in the paper). The motivation for considering the latter configuration is that it may be much easier to fabricate, and provides further degrees of freedom in the design of the metamaterial. In addition, the phenomenon of negative refraction is confirmed with full-wave commercial software that models the incidence of a Gaussian beam on a finite width metamaterial slab.

A. Multilayered mushroom-type metamaterial

As a first example, we consider a multilayered mushroom structure formed by five identical patch arrays separated by four dielectric layers perforated with vias (the geometry of a generic structure is shown in Fig. 1). Each patch array has the period $a = 2$ mm and gap $g = 0.2$ mm, and each dielectric slab is of thickness 2 mm with permittivity 10.2. The period of the vias is 2 mm with a radius of 0.05 mm. The plasma frequency $(f_p/\sqrt{\varepsilon_h})$ of the WM slab is approximately at 12.15 GHz. The transmission properties (magnitude and phase) of the structure based on the local and

nonlocal homogenization models for a TM-polarized plane wave incident at 45 degrees are shown in Fig. 2. It is seen that the results of the two models are in good agreement with the full-wave simulations results obtained with CST Microwave Studio^{TM},[21] especially in the region below the plasma frequency. In the vicinity of the plasma frequency the local model shows spurious resonances in a very narrow frequency band. The spurious resonances appear because of the singularity in Eq. 14, where $\varepsilon_{zz}^{loc} = 0$ at the plasma frequency. For the mushroom structures studied in Refs. 13 and 14, it has been shown that the spatial dispersion effects in the wire medium can be suppressed (or significantly reduced) by loading vias with a capacitive grid of metallic patches. This results in a nearly uniform current along the vias, i.e., $d/dz \approx 0$ or in the spectral domain $k_z \approx 0$. Under this condition the nonlocal dielectric function Eq. 1 reduces to the local dielectric function Eq. 11. Consistent with these findings and with Refs. 15 and 16, the results of Fig. 2 (showing an excellent agreement of the results of nonlocal and local homogenization models, even above the plasma frequency) support that for the considered geometry of a multilayered metamaterial (Fig. 1) the effects of spatial dispersion are suppressed and below the plasma frequency it behaves as a uniaxial continuous ENG material loaded with patch arrays.

In order to study the emergence of negative refraction in the multilayered mushroom structure we use the formalism proposed in Ref. 7, which is based on the analysis of the variation in the phase of $T(\omega, k_x)$ (transmission coefficient for a plane wave characterized by the transverse wave number k_x) of the metamaterial slab with the incident angle θ_i. Specifically, it was shown in Ref. 7, that for an arbitrary material slab excited by a quasiplane wave, apart from the transmission magnitude, the field at the output plane differs from the field at the input plane by a spatial shift Δ [see inset in Fig. 3(b)], given by $\Delta = d\varphi/dk_x$, where $\varphi = \arg T$. The transmission angle can be obtained as $\theta_t = \tan^{-1} \Delta/L$ (L is the thickness of the planar material slab). Thus, negative refraction occurs when Δ is negative, i.e., when φ decreases with the angle of incidence θ_i. It should be noted that the calculation of spatial shift is more accurate when there is a smooth variation in the magnitude of the transfer function $T(\omega, k_x)$.

Figure 3 demonstrates the behavior of the magnitude and phase of the transmission coefficient versus the angle of incidence at the frequency of 11 GHz ($\varepsilon_{zz}^{loc} = -2.23$). It can be seen that the phase of transmission coefficient decreases with an increase in the incident angle, which indicates unequivocally the emergence of negative refraction. The total transmission occurs at the incident angle of 32.73 degrees, and the calculated spatial shift (using finite differences for the calculation of $d\varphi/dk_x$) at this angle is $\Delta = -1.02\lambda_0$ (λ_0 is the free-space wavelength at 11 GHz) with the electrical thickness of the metamaterial slab equal to $L = 0.29\lambda_0$. The calculated transmission angle is -73.8 degrees, thus demonstrating a strong negative refraction. This shows that the multilayered mushroom-type structure

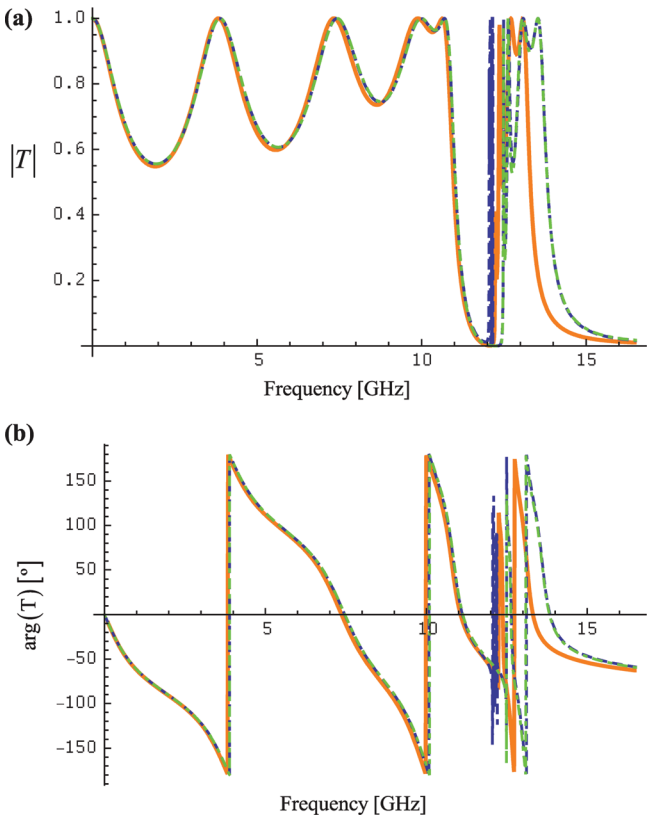

FIG. 2. (Color online) Comparison of local (blue dashed lines), nonlocal (green dot-dashed lines), and full-wave CST results (orange full lines) for the five-layered (five patch arrays with four WM slabs) structure excited by a TM-polarized plane wave incident at 45 degrees. (a) Magnitude of the transmission coefficient. (b) Phase of the transmission coefficient.

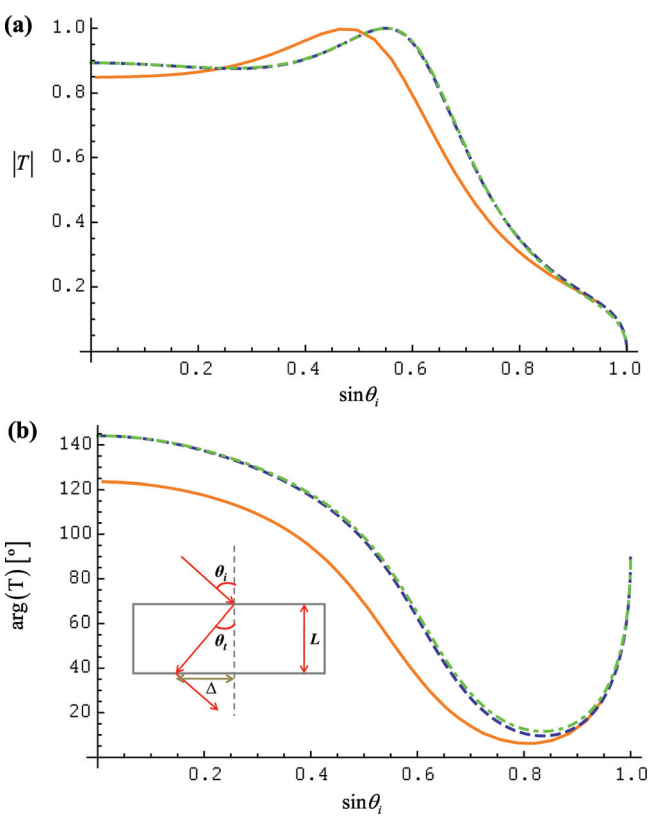

FIG. 3. (Color online) Comparison of local (blue dashed lines), nonlocal (green dot-dashed lines), and full-wave CST results (orange full lines) for the five-layered (five patch arrays with four WM slabs) structure as a function of the incident angle of a TM-polarized plane wave. (a) Magnitude of the transmission coefficient. (b) Phase of the transmission coefficient.

enables negative refraction at an interface with air, when the effects of spatial dispersion in the WM are suppressed.

Next, we consider the dependence of the negative refraction on the number of layers of the multilayered structure. Specifically, we have calculated the spatial shift Δ and the transmission angle θ_t as a function of the incident angle θ_i, for a different number of identical layers of the mushroom structure (with the same dimensions as considered in the previous example). Figure 4 shows the analytical results based on the local homogenization model at the frequency of 11 GHz. It is evident that there is an increase in the absolute value of the spatial shift with the increase in the number of layers (substantial increase in the overall length of the metamaterial). However, there is no significant change in the angle of transmission (negative refraction). The calculated Δ and θ_t for a different number of patch arrays with the incident angle tuned to achieve maximum transmission are listed in Table I.

It is worth considering the effect of the negative refraction with respect to the operating frequency. We have calculated the spatial shift Δ and the transmission angle θ_t as a function of the incidence angle θ_i at different frequencies for the six-layered structure (six identical patch arrays with five identical WM slabs) with the same dimensions used in the previous examples. The results of the local homogenization model are depicted in Fig. 5. It can be seen that the phenomenon of negative refraction is observed over a wide frequency band below the plasma frequency.

Although negative refraction is observed over a wide frequency band, its strength becomes gradually weaker with the

TABLE I. Characterization of the negative refraction with an increase in the number of identical layers.

N grids	Δ/λ_0	L/λ_0	θ_i (deg)	θ_t (deg)
2	−0.22	0.074	22.96	−71.4
3	−0.45	0.148	29.09	−71.9
4	−0.7	0.22	31.33	−72.55
5	−1.0	0.29	32.73	−73.8
6	−1.30	0.364	34.68	−74.62
7	−1.73	0.438	35.76	−75.79

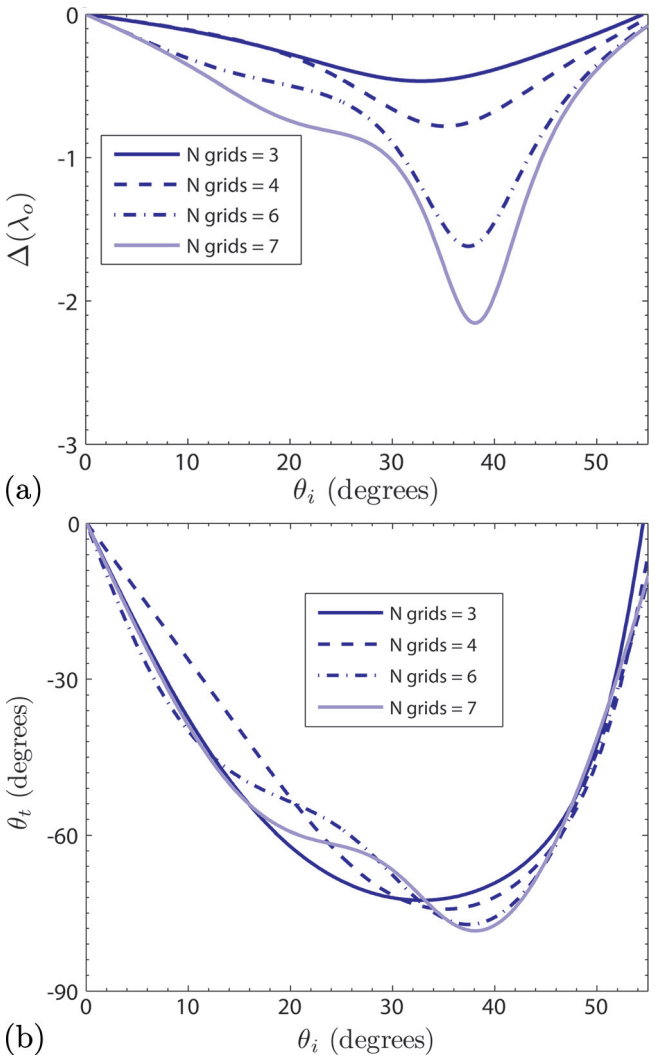

FIG. 4. (Color online) (a) Spatial shift Δ and (b) transmission angle θ_t as a function of the incident angle θ_i of a TM-polarized plane wave calculated for the multilayered structure with a different number of layers.

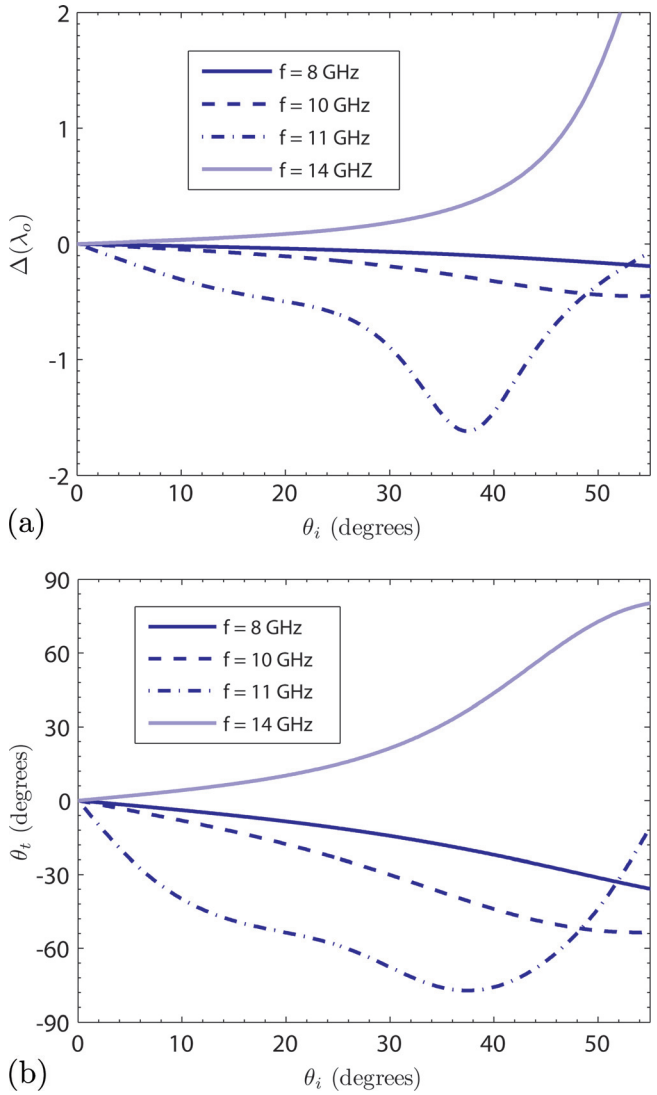

FIG. 5. (Color online) (a) Spatial shift Δ and (b) transmission angle θ_t for the six-layered (six patch arrays and five WM slabs) structure as a function of the incident angle θ_i of a TM-polarized plane wave calculated at different frequencies.

decrease in the frequency of operation. For instance, at the frequency of 11 GHz, the maximum negative refraction angle is −74.62 degrees, and it decreases to −34.52 degrees with the decrease in the operating frequency to 8 GHz. However, when one operates above the plasma frequency ($\varepsilon_{zz}^{loc} > 0$), the mushroom structure exhibits positive refraction. It is apparent that the frequency range where one can observe the negative refraction can be shifted by changing the plasma frequency. It should be noted that the negative refraction properties of the proposed multilayered mushroom structure can be controlled by the geometrical parameters. For example (results are not reported here), an increase in the radius of the vias increases the plasma resonance frequency, and, therefore, in order to operate in the negative refraction regime (close to the plasma resonance) the frequency has to be increased. This may, however, result in the conditions when the homogenization is no longer valid. Also, the requirement that the patches in different layers are connected through the metallic vias creates obvious difficulties in the practical realization of a structure with a large number of layers (due to technological difficulties in the alignment of the layers in the stacked structure, and in the realization of long vias of small radius). In the next section we propose an alternative structure that overcomes these problems and provides one extra degree of freedom to control the negative refraction angle of the metamaterial without changing its structural properties.

B. Multilayered mushroom-type metamaterial with air gaps

Here we consider a mushroom-type metamaterial with air gaps, as shown in Fig. 6. The structure is formed by several two-sided mushroom slabs (with two symmetric patch arrays connected with vias) separated by air gaps. Here, a is the period of the patches and the vias, g is the gap between the patches, h is the thickness of the dielectric layer between the patch arrays, ε_h is the permittivity of the dielectric slab, h_a is the thickness of the air gap, and r_0 is the radius of the vias.

We consider the case of a structure formed by two mushroom slabs with an air gap. The dimensions are the same as used in the previous examples, and the thickness of the air gap is 2 mm. The transmission response of the structure based on the local and nonlocal homogenization models for the TM-polarized plane wave incident at 45 degrees is shown in Fig. 7. It is seen that there is a good agreement between the results of the two models. Also, the homogenization results agree reasonably well with the full-wave simulation results obtained with HFSS,[22] especially in the region below the plasma frequency.

We have characterized the negative refraction using the same procedure as in the previous section. It can be seen from Fig. 8, that at the operating frequency of 11 GHz, there is a monotonic decrease in the angle $\varphi = \arg T$ with the variation in the incidence angle, except for large incident angles corresponding to the rapid change in the transmission magnitude. This clearly indicates that the multilayered mushroom metamaterial with air gaps enables negative refraction. The calculated negative spatial shift at the incident angle of 23.3 degrees corresponding to the transmission maximum is

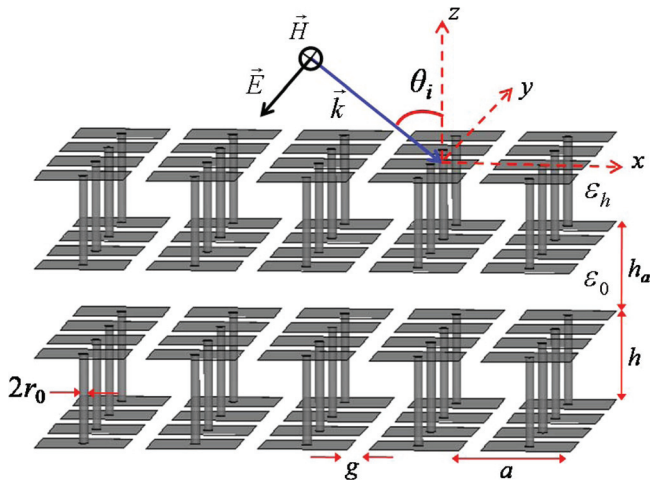

FIG. 6. (Color online) 3D view of the mushroom-type metamaterial formed by including the air gap (without vias) in between two-layered (paired) mushrooms.

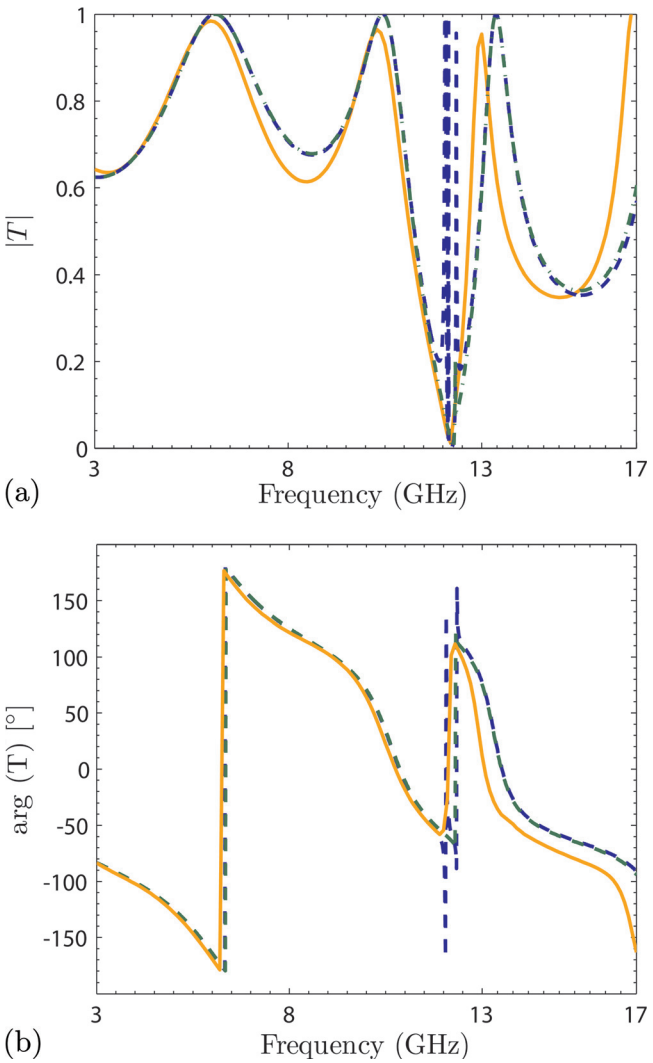

FIG. 7. (Color online) Comparison of local (blue dashed lines), nonlocal (green dot-dashed lines), and full-wave HFSS results (orange full lines) for the multilayered mushroom structure with an air gap excited by a TM-polarized plane wave incident at 45 degrees. (a) Magnitude of the transmission coefficient. (b) Phase of the transmission coefficient.

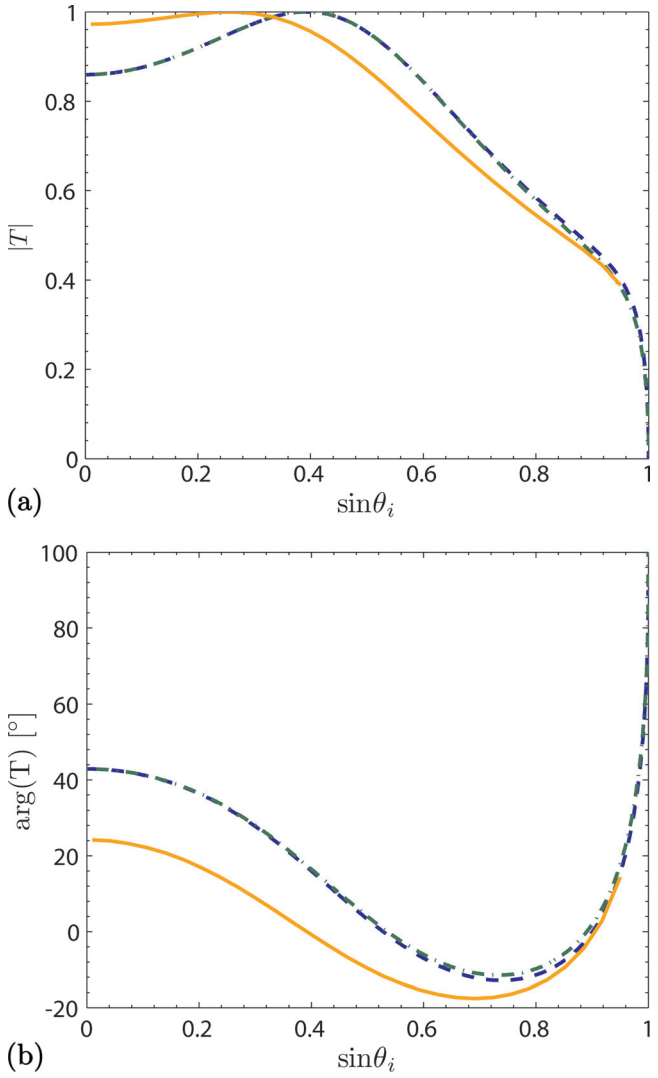

FIG. 8. (Color online) Comparison of local (blue dashed lines), nonlocal (green dot-dashed lines), and full-wave CST results (orange full lines) for two double-sided mushroom slabs separated by an air gap as a function of the incident angle of a TM-polarized plane wave. (a) Magnitude of the transmission coefficient. (b) Phase of the transmission coefficient.

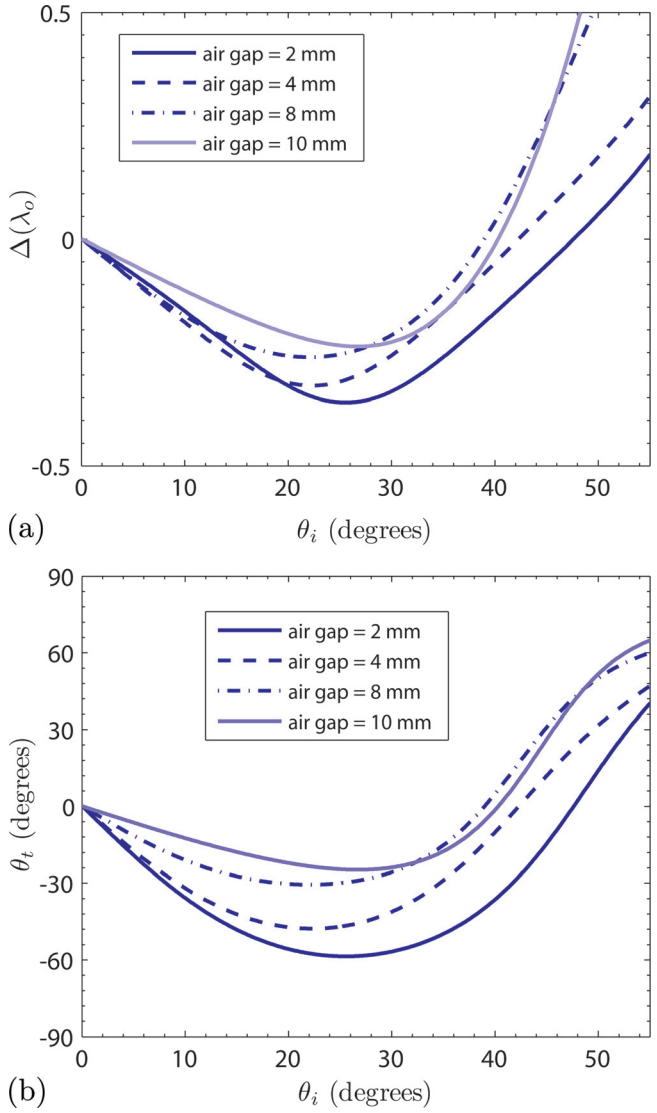

FIG. 9. (Color online) (a) Spatial shift Δ and (b) transmission angle θ_t as a function of the incident angle θ_i of a TM-polarized plane wave calculated for the multilayered structure with the varying thickness of the air gap h_a.

$\Delta = -0.35\lambda_0$. The electrical length of the multilayered structure at 11 GHz is $L = 0.22\lambda_0$, and the calculated transmission angle is -58.15 degrees. It is interesting, that despite the presence of an air region (characterized by a positive refraction), the structure still exhibits quite significant negative refraction.

In order to further characterize the dependence of negative refraction on the thickness of the air gap h_a, we have calculated the spatial shift Δ and the transmission angle θ_t as a function of the incidence angle θ_i, at the operating frequency of 11 GHz. The results are depicted in Fig. 9, and are obtained based on the local homogenization model. It can be observed that there is a steady decrease in the calculated negative spatial shift with the increase in the thickness of the air gap. This is due to the increased positive spatial shift in the air region (with the increase of the air gap). Moreover, there is a significant decrease in the negative refraction angle. The calculated spatial shift Δ and the angle of transmission θ_t for different values of the air gap h_a with the incident angle θ_i of the transmission maximum are given in Table II. It is evident that the incident angle remains almost the same, however, the corresponding transmission angle decreases significantly. Consequently, it is possible to control the negative refraction angle by varying the thickness of the air gap. The proposed geometry is of great practical interest, because of the ease in fabrication. Interestingly, the structure exhibits negative refraction only for moderate angles (<45 degrees) of incidence. Considering the fact that the positive spatial shift in the air region is dependent on the angle of incidence, for large incident angles the suffered positive spatial shift in the

TABLE II. Characterization of the negative refraction as a function of the thickness of the air gap h_a.

h_a (mm)	Δ/λ_0	L/λ_0	θ_i (deg)	θ_t (deg)
2	−0.35	0.22	23.3	−58.15
4	−0.32	0.29	22.9	−47.73
6	−0.29	0.37	22.8	−38.59
8	−0.26	0.44	22.1	−30.61
10	−0.22	0.51	21.9	−23.32

air region dominates the negative spatial shift in the wire medium, thus creating a positive refraction.

It is interesting to see if the negative refraction is observed over a wide frequency band. We have calculated Δ and θ_t as a function of the incident angle at different frequencies, and the analytical results based on the local model are shown in Fig. 10. It can be seen that there is a rapid decrease in the strength of the negative refraction with the decrease in the operating frequency (below the plasma frequency). In fact (as discussed in the case without air gaps), the negative refraction becomes gradually weaker away from the plasma frequency, i.e., the absolute value of the negative spatial shift decreases. Consequently, in this case the positive spatial shift in the air region dominates, thus reducing the frequency band for the emergence of negative refraction.

C. Gaussian beam excitation

To further confirm the predicted phenomenon of negative refraction based on the homogenization models, we have simulated the response of the metamaterial structures excited by a Gaussian beam using CST Microwave Studio.[21] In the simulation setup, the structure is assumed to be periodic along y with the period a (equal to the period of the patch array),

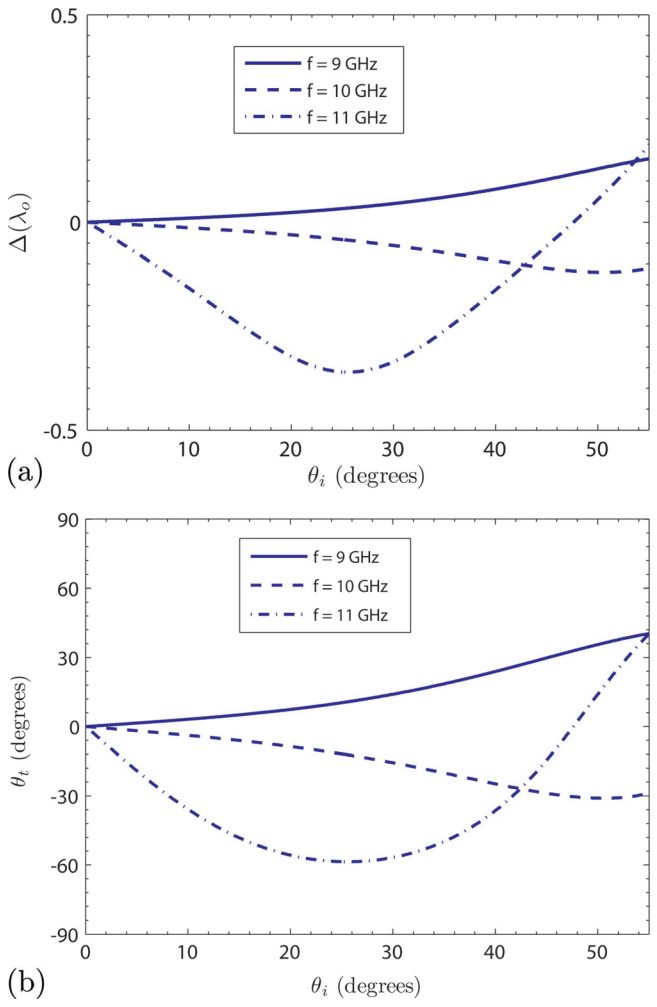

FIG. 10. (Color online) (a) Spatial shift and (b) transmission angle for the multilayered structure with an air gap of 2 mm as a function of incident angle of a TM-polarized plane wave calculated at different frequencies.

and is finite along x with the width $W_x = 90a$. The considered Gaussian beam field distribution is independent on the y-coordinate. We excite simultaneously 10 adjacent waveguide ports, with the electric width of the each port being $0.3\lambda_0$ at the design frequency. The amplitude and phase of each waveguide are chosen such that the wave radiated by the port array mimics the profile of a Gaussian beam and propagates along a desired direction θ_i in the x-z plane. The cases of mushroom slabs with and without air gaps are considered, with the same geometrical parameters used in the previous examples. In the simulation, the effects of losses are taken into account: the metallic components are modeled as copper metal ($\sigma = 5.8 \times 10^7 \mathrm{S/m}$), and a loss tangent of $\tan\delta = 0.0015$ is considered in dielectric substrates (RT/duroid 6010LM).

The results obtained with the CST Microwave Studio are shown in Fig. 11. The snapshot ($t = 0$) of the amplitude of the magnetic field H_y of the Gaussian beam incident at 19 degrees is shown in Fig. 11(a). The Gaussian beam-waist is approximately $1.6\lambda_0$ at the operating frequency of 11 GHz. Figure 11(b) shows the snapshot of the amplitude of H_y in the vicinity of the metamaterial structure with a 2 mm air gap (formed by two mushroom slabs with an air gap as shown in Fig. 6) illuminated by the Gaussian beam incident at 19 degrees. It can be observed that the transmitted beam suffers a negative spatial shift, demonstrating a significant negative refraction inside of the metamaterial. Similar results are depicted in Fig. 11(d) with the Gaussian beam incident at 30 degrees. The simulation results are qualitatively consistent with the theoretical values (predicted by the homogenization models) for the spatial shift $\Delta = -0.31\lambda_0$ and $\Delta = -0.33\lambda_0$, calculated with the incident angles of 19 degrees and 30 degrees, respectively. Figure 11(c) depicts the case of the Gaussian beam incident at 19 degrees on the metamaterial structure formed by three mushroom slabs with two air gaps. The theoretical value of the spatial shift for the configuration in Fig. 11(c) is $\Delta = -0.44\lambda_0$, while that for the case shown in Fig. 11(b) is $\Delta = -0.31\lambda_0$. However, it should be noted that the negative refraction angle remains almost the same [with the predicted theoretical values of -54.63 degrees and -50.63 degrees for the cases (b) and (c), respectively].

The magnetic field in the vicinity of the five-layered structure without air gaps (with the geometry shown in Fig. 1) for the Gaussian beam incident at 32 degrees is depicted in Fig. 11(e). It is seen that the transmitted beam suffers a large negative spatial shift, thus exhibiting a strong negative refraction, and the simulation results are consistent with the ones reported in Refs. 15 and 16. The negative spatial shift in the metamaterial is a significant fraction of the wavelength.

It should be noted that due to computational limitations the Gaussian beam cannot be treated exactly as a quasiplane wave (since its beam-width is marginally larger than $1.5\lambda_0$). Thus, the analytical results based on the homogenization models are qualitatively accurate but quantitatively approximate in modeling a realistic finite metamaterial with the Gaussian beam excitation.

IV. CONCLUSION

In this paper, we investigated multilayered mushroom-type structures as bulk metamaterials which enable strong

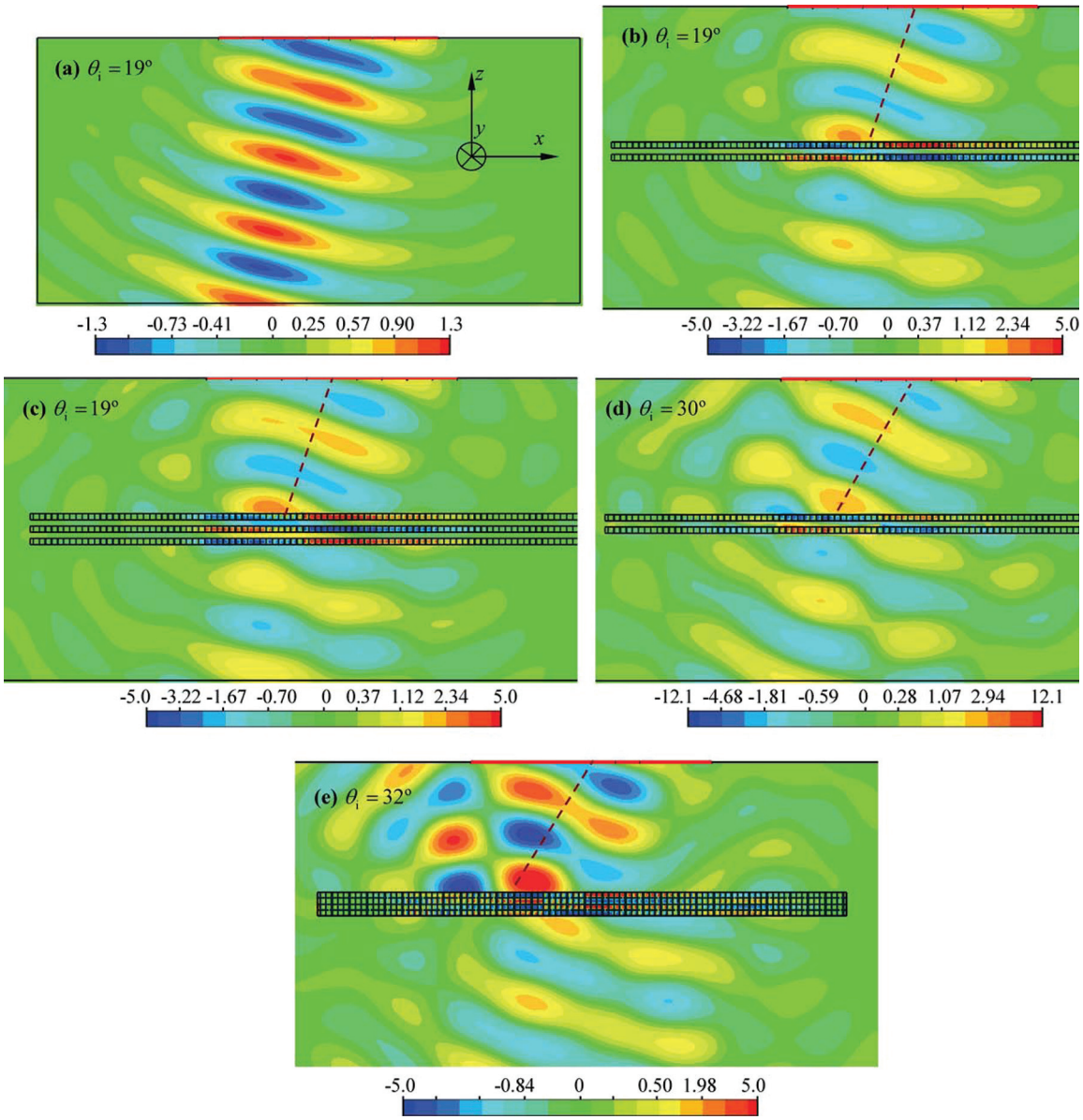

FIG. 11. (Color online) CST Microwave Studio simulation results showing the snapshot ($t = 0$) of the magnetic field H_y excited by a Gaussian beam: (a) incident beam with $\theta_i = 19$ degrees (no metamaterial slab), (b) two mushroom slabs with an air gap for an angle of incidence $\theta_i = 19$ degrees, (c) three mushroom slabs with two air gaps for an angle of incidence $\theta_i = 19$ degrees, (d) two mushroom slabs with an air gap for an angle of incidence $\theta_i = 30$ degrees, and (e) five-layered structure (without air gaps with the geometry shown in Fig. 1) for an angle of incidence $\theta_i = 32$ degrees. The operating frequency for all the cases is 11 GHz and the thickness of the air gap is 2 mm.

negative refraction. The transmission properties of the metamaterials are studied based on the local and nonlocal homogenization models.

Consistent with Refs. 15 and 16, it was shown that the multilayered mushroom-type metamaterial behaves as a local (with no spatial dispersion) uniaxial ENG material periodically loaded with patch arrays. The negative refraction is observed over a wide frequency band below the plasma frequency, and is accurately predicted by the homogenization models. The strength of the negative refraction decreases gradually when we operate away from the plasma frequency. In addition, we proposed a modified structure where the mushroom slabs are separated by air gaps. It was shown that this configuration also exhibits significant negative refraction, and enables the control of the negative transmission angle by varying the thickness of the air gap without changing the structural properties of the metamaterial. Such configuration is of great practical importance because of the ease in fabrication. It is planned to obtain the experimental verification of the proposed configurations, which is the scope of future work.

The observed phenomenon of negative refraction was qualitatively verified with the Gaussian beam excitation using CST Microwave Studio.

APPENDIX

The tangential electric and magnetic fields given by Eqs. 2 and 3 across the patch interfaces (at the planes $z = z_0 = 0, -h, -2h, ..., -L$) can be related in the matrix form using the two-sided impedance boundary conditions (Eqs. 5 and 6),

$$\begin{bmatrix} E_x \\ \eta_0 H_y \end{bmatrix}_{z=z_0^-} = Q \begin{bmatrix} E_x \\ \eta_0 H_y \end{bmatrix}_{z=z_0^+}, \tag{A1}$$

where Q is the transfer matrix across the plane of patches,

$$Q = \begin{bmatrix} 1 & 0 \\ y_g & 1 \end{bmatrix}. \tag{A2}$$

In Eq. A2, y_g is the normalized admittance of the patch grids given by Eq. 7. The transfer matrix for the propagation in the WM slab between the two adjacent patch grids used in the nonlocal homogenization model is obtained by substituting Eqs. 2 and 4 in the ABC (Eq. 8), and relating the tangential electric and magnetic field components at the plane $z = (z_0 - h)^+$ to the fields at the plane $z = z_0^-$. Following Ref. 20, the transfer matrix is as follows:

$$\begin{bmatrix} E_x \\ \eta_0 H_y \end{bmatrix}_{z=(z_0-h)^+} = P \cdot \begin{bmatrix} E_x \\ \eta_0 H_y \end{bmatrix}_{z=z_0^+}, \tag{A3}$$

where the matrix P is

$$P = \begin{bmatrix} p_{11} & p_{12} \\ p_{21} & p_{22} \end{bmatrix} \tag{A4}$$

with the matrix elements:

$$p_{11} = p_{22} = \frac{(\varepsilon_h - \varepsilon_{zz}^{\mathrm{TM}})\gamma_{\mathrm{TM}} \sinh(\gamma_{\mathrm{TM}} h)\cosh(\gamma_{\mathrm{TEM}} h) + \varepsilon_{zz}^{\mathrm{TM}} \gamma_{\mathrm{TEM}} \cosh(\gamma_{\mathrm{TM}} h)\sinh(\gamma_{\mathrm{TEM}} h)}{(\varepsilon_h - \varepsilon_{zz}^{\mathrm{TM}})\gamma_{\mathrm{TM}} \sinh(\gamma_{\mathrm{TM}} h) + \varepsilon_{zz}^{\mathrm{TM}} \gamma_{\mathrm{TEM}} \sinh(\gamma_{\mathrm{TEM}} h)}, \tag{A5}$$

$$p_{12} = -\frac{1}{k_0} \frac{j\gamma_{\mathrm{TEM}}\gamma_{\mathrm{TM}} \sinh(\gamma_{\mathrm{TM}} h)\sinh(\gamma_{\mathrm{TEM}} h)}{(\varepsilon_h - \varepsilon_{zz}^{\mathrm{TM}})\gamma_{\mathrm{TM}} \sinh(\gamma_{\mathrm{TM}} h) + \varepsilon_{zz}^{\mathrm{TM}} \gamma_{\mathrm{TEM}} \sinh(\gamma_{\mathrm{TEM}} h)}, \tag{A6}$$

$$p_{21} = jk_0 \left\{ \frac{2(\varepsilon_h - \varepsilon_{zz}^{\mathrm{TM}})\varepsilon_{zz}^{\mathrm{TM}}[-1 + \cosh(\gamma_{\mathrm{TM}} h)\cosh(\gamma_{\mathrm{TEM}} h)]}{(\varepsilon_h - \varepsilon_{zz}^{\mathrm{TM}})\gamma_{\mathrm{TM}} \sinh(\gamma_{\mathrm{TM}} h) + \varepsilon_{zz}^{\mathrm{TM}} \gamma_{\mathrm{TEM}} \sinh(\gamma_{\mathrm{TEM}} h)} + \frac{\sinh(\gamma_{\mathrm{TEM}} h)\sinh(\gamma_{\mathrm{TM}} h)\left[(\varepsilon_h - \varepsilon_{zz}^{\mathrm{TM}})^2 \frac{\gamma_{\mathrm{TM}}}{\gamma_{\mathrm{TEM}}} + (\varepsilon_{zz}^{\mathrm{TM}})^2 \frac{\gamma_{\mathrm{TEM}}}{\gamma_{\mathrm{TM}}}\right]}{(\varepsilon_h - \varepsilon_{zz}^{\mathrm{TM}})\gamma_{\mathrm{TM}} \sinh(\gamma_{\mathrm{TM}} h) + \varepsilon_{zz}^{\mathrm{TM}} \gamma_{\mathrm{TEM}} \sinh(\gamma_{\mathrm{TEM}} h)} \right\}. \tag{A7}$$

The global transfer matrix for the entire multilayered structure can be obtained as a product of the corresponding transfer matrices,

$$M_G = Q_0 \cdot P \cdot Q \cdot \cdots \cdot P \cdot Q_0, \tag{A8}$$

where Q_0 is the transfer matrix across the plane of patches for the upper and the lower external grids and Q is the transfer matrix for all internal grids.

The global transfer matrix for the local model is the same as that of the nonlocal model, except for the transfer matrix P. The transfer matrix P (for the propagation in the WM slab), is obtained by matching the fields at the interfaces $z = (z_0 - h)^+$ and $z = z_0^-$ in a similar form as Eq. A3, and is expressed as follows:

$$P = \begin{bmatrix} \cosh(\gamma h) & \left(\frac{\gamma}{jk_0\varepsilon_h}\right)\sinh(\gamma h) \\ \left(\frac{jk_0\varepsilon_h}{\gamma}\right)\sinh(\gamma h) & \cosh(\gamma h) \end{bmatrix}. \tag{A9}$$

[1] V. G. Veselago, Sov. Phys. USP. **10**, 509 (1968).
[2] A. Schuster, *An introduction to the Theory of Optics* (Edward Arnold, London, 1904), p. 317.
[3] L. I. Mandelshtam, Complete Collection of Works **5**, 428–467 (1944) (in Russian).
[4] D. R. Smith and D. Schurig, Phys. Rev. Lett. **90**, 077405 (2003).
[5] D. R. Smith, D. Schurig, J. J. Mock, P. Kolinko, and P. Rye, Appl. Phys. Lett. **84**, 2244 (2004).
[6] Q. Cheng, R. Liu, J. J. Mock, T. J. Cui, and D. R. Smith, Phys. Rev. B. **78**, 121102 (2008).
[7] M. G. Silveirinha, Phys. Rev. B. **79**, 153109 (2009).
[8] E. Cubukcu, K. Aydin, E. Ozbay, S. Foteinopoulou, and C. M. Soukoulis, Nature **423**, 604 (2003).
[9] J. Yao, Z. Liu, Y. Liu, Y. Wang, C. Sun, G. Bartal, A. M. Stacy, and X. Zhang, Science **321**, 930 (2008).
[10] Y. Liu, G. Bartal, and X. Zhang, Opt. Express **16**, 15439 (2008).
[11] P. A. Belov, R. Marques, S. I. Maslovski, I. S. Nefedov, M. Silveirinha, C. R. Simovski, and S. A. Tretyakov, Phys. Rev. B. **67**, 113103 (2003).
[12] A. Demetriadou and J. B. Pendry, J. Phys.: Condens. Matter **20**, 295222 (2008).
[13] O. Luukkonen, M. G. Silveirinha, A. B. Yakovlev, C. R. Simovski, I. S. Nefedov, and S. A. Tretyakov, IEEE Trans. Microwave Theory and Tech. **57**, 2692 (2009).
[14] A. B. Yakovlev, M. G. Silveirinha, O. Luukkonen, C. R. Simovski, I. S. Nefedov, and S. A. Tretyakov, IEEE Trans. Microwave Theory and Tech. **57**, 2700 (2009).
[15] A. B. Yakovlev, M. G. Silveirinha, and C. S. R. Kaipa, in *Proceedings IEEE MTT 2010 International Microwave Symposium*, 173 (2010).
[16] M. G. Silveirinha and A. B. Yakovlev, Phys. Rev. B. **81**, 233105 (2010).
[17] O. Luukkonen, C. R. Simovski, G. Granet, G. Goussetis, D. Lioubtchenko, A. V. Raisanen, and S. A. Tretyakov, IEEE Trans. Antennas Propagat. **56**, 1624 (2008).
[18] M. G. Silveirinha, C. A. Fernandes, and J. R. Costa, IEEE Trans. Antennas Propagat. **56**, 405 (2008).
[19] M. G. Silveirinha, C. A. Fernandes, and J. R. Costa, New J. Phys. **10**, 053011 (2008).
[20] S. I. Maslovski and M. G. Silveirinha, Phys. Rev. B. **80**, 245101 (2009).
[21] CST Microwave Studio, **2009**, CST GmbH, http://www.cst.com.
[22] HFSS: High Frequency Structure Stimulator based on Finite Element Method, Ansoft Corporation, http://www.ansoft.com.